Higher performing older adults upregulate brain signal variability in response to feature-rich sensory input

Douglas D. Garrett[1,2], Samira Epp[1,2], Maike Kleemeyer[2], Ulman Lindenberger[1,2], and Thad A. Polk[3]

[1]Max Planck UCL Centre for Computational Psychiatry and Ageing Research, Berlin/London; [2]Center for Lifespan Psychology, Max Planck Institute for Human Development, Lentzeallee 94, 14195 Berlin, Germany; [3]Department of Psychology, University of Michigan, Ann Arbor, MI, USA.

Abstract

Differentiation of brain signal variability across different cognitive states has been hypothesized to facilitate adaptation to changing task demands, but why signal variability should be higher or lower on a given task remains unknown. We hypothesized that the level of brain signal variability should mirror the feature density of sensory input, especially in high performers. To test these hypotheses, we had 46 healthy older adults passively view face and house stimuli during fMRI. We first used a computational model of the ventral visual stream (HMAX) to decode the feature content of all face and house images seen by participants; model results revealed that house images were much more feature-rich than faces, particularly for V1- and V2-like model layers. Using fMRI, we then found that participants whose V1/V2 brain signal variability increased the most in response to more feature-rich visual input (houses vs. faces) also exhibited faster and more stable behavioral performance on a comprehensive battery of offline visual tasks. We conclude that the ability to align visuocortical signal variability to the density of visual input may mark heightened trait-level behavioral performance in older adults.

Brain signal variability upregulates in response to more feature-rich sensory input in high performers

Numerous studies have found that cognitive and brain functions become less "differentiated" as humans age. For example, neural responses to different stimulus input tend to become more similar with increasing age[1,2]. Neural differentiation is often measured by training a classifier to distinguish trial aggregated or response averaged neural activation patterns associated with different cognitive states (e.g., faces vs. houses in ventral visual cortex) and then measuring the classifier's accuracy in decoding untrained activation patterns. However, an emerging approach has examined neural differentiation using moment-to-moment brain signal variability to characterize different cognitive states. Our past work shows that older, poorer performing adults express more similar within-person levels of neural variability across task types and brain regions than younger, higher performers[3-6]. Indeed, we hypothesize generally that the differentiation of brain signal variability levels across varying cognitive states may enable an organism to flexibly and optimally adapt to a host of environmental challenges[3].

However, why should signal variability be higher on one task and lower on another? We, and others, have postulated that brain signal variability may be tuned to reflect the dynamics or differentiation of stimulus input (and associated level of stimulus "uncertainty")[3,6-10]. For example, some evidence suggests that early visual regions are actively suppressed in response to expected (or more common) stimuli, and exhibit a more dynamic response to unexpected (or more differentiated) stimuli[11-13]. Thus, more varied, differentiated visual input could presumably invoke brain responses with greater dynamic range. Notably, computational and animal work[10] suggests that a wider range of image features (feature richness) could yield more varied neural responses in visual cortex. However, to our knowledge, evidence for this effect is lacking in humans. In particular, individual differences in the ability to tune signal variability to the level of stimulus feature density, and the possible behavioral consequences of this ability, have not been systematically investigated. A metabolically and computationally "optimal" brain should conceivably limit resource allocation when stimulus input is more reducible and/or predictable[14], and it should upregulate dynamic range to the extent that more resource intensive processing is required (e.g., to encode more varied sources of sensory input). At its core, modulation of brain signal variability may reflect one's ability to tune to the dynamics of the external world. We would therefore expect that people who exhibit greater modulation of variability should also exhibit better cognitive performance overall, as such individuals would be more adaptable to varied types of stimulus input in general.

In the present study, we used a computational model of the ventral visual stream (HMAX) to quantify the feature density of face and house stimuli. These same stimuli were also passively viewed by older adults while brain signal variability was measured during fMRI. We hypothesized that (1) the modulation of brain signal variability in visual cortex would mirror the feature density of visual input, and that (2) greater upregulation in signal variability for stimuli with greater feature density would be associated with better cognitive performance across a battery of visuo-cognitive measures.

RESULTS

Quantifying the feature density of visual input using a feedforward computational model of the ventral visual stream

To gauge the feature density of visual input (for face and house stimuli), we used a biologically-inspired feedforward computational model (HMAX)[15-18]. Its output consists of a hierarchy of four layers intended to model the function of different brain regions within the ventral visual stream (see Figure 1). The S1 and C1 layers are thought to reflect processing from simple and complex cells in V1/V2, whereas S2 and C2 layers are intended to reflect simple and complex composite feature cells from V2/V4 [16,17].

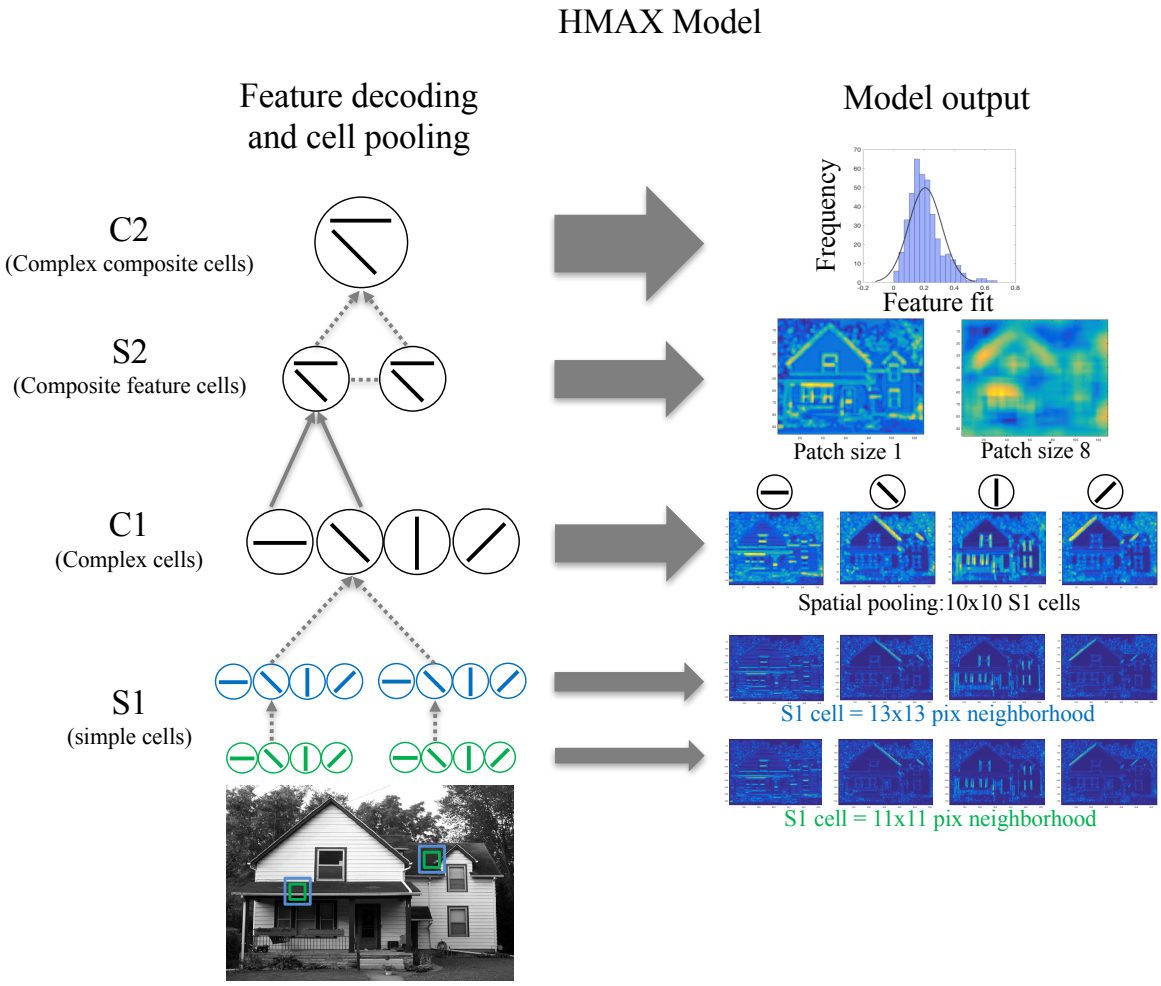

Figure 1: Visualization of the HMAX model of ventral visual cortex (see Riesenhuber et al. (1999) and Serre et al. (2007)). Left panel ("Feature decoding and cell pooling"): the model is sketched. Two example house image locations and neighborhood sizes are shown (green/blue boxes), from which all orientations are decoded. At the S1 (simple cell) layer, these locations are convolved with different Gabor filter sizes within each orientation (here, two filter (neighborhood) sizes of 11x11 (in green) and 13x13 pixels (in blue), and 4 orientations, are shown). At the C1 layer, the model takes the max (dotted paths) simultaneously over both filter sizes and over a pool of S1 cells (here, 10x10 cells) for each orientation separately. The S2 layer represents hybrid features estimated via weighted sum (solid grey paths) after comparison of image features to 400 prototypical features from an external image set, separately for a series of C1 cell neighborhood sizes within each scale band (example scale band 2 is shown). Finally, layer C2 represents the max taken over all S2 cells to generate an aggregated "fit" (inverse Euclidean distance) of image features to the 400 feature prototypes. Right panel ("Model output"): The output of these example steps for the entire image is shown, with warmer colors representing better fits to each orientation (layers S1 and C1) and prototype (layer S2).

HMAX allows for quantification of the feature density (richness) of within-image spatial features in several ways. We focused our analyses on C1 and C2 layers as aggregate representations of single and composite feature cells for V1/V2 and V2/V4 respectively[16] (see Figure 1 and Methods). At layer C1, "features" are represented by a target set of four spatial orientations (-45°, 0°, 45°, 90°) within and across different filter and neighborhood ("receptive field") sizes (see Methods). The median C1 fit value provides a measure of how

often a given orientation occurred within an image. Model results indicated that each spatial orientation occurred significantly more often for house than for face stimuli across all filter bands (i.e. receptive field sizes; Figure 2, left panel). Interestingly, condition separation at C1 appeared to increase with increasing scale band (receptive field) size (Figure 3, left panel), suggesting that face features are more "reducible" relative to houses as receptive field size grows in V1/V2 cells.

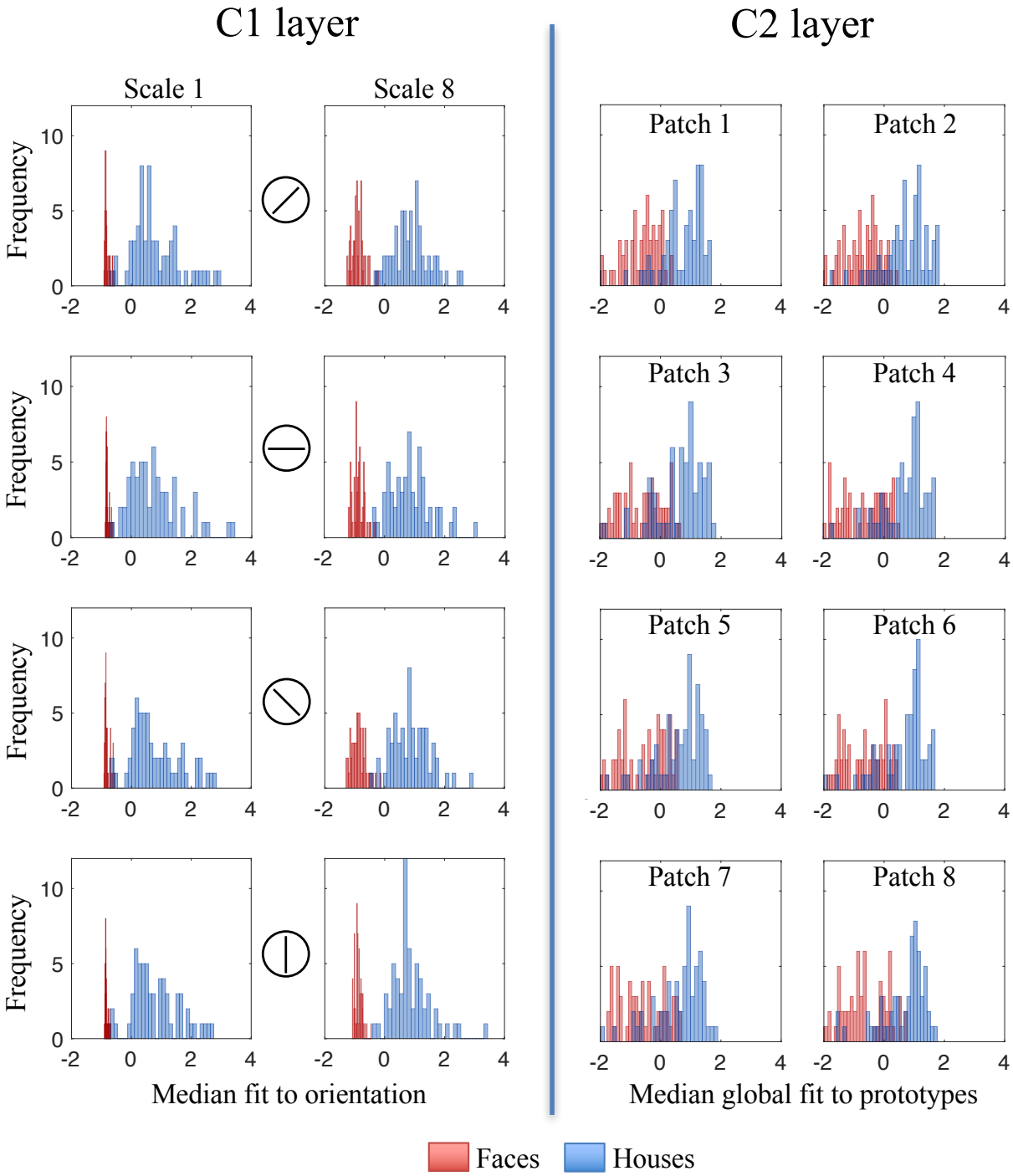

Figure 2: C1 and C2 distributions for face and house stimuli. All 60 unique images per condition from the fMRI stimulus set were submitted to the model. At the C1 layer (left), the median of each C1 map is shown, averaging over all locations within-image, for the smallest and largest scale bands (1 and 8) and each orientation separately. At the C2 layer (right), the median within-image fit to a library of 400 feature prototypes is displayed for each of eight neighborhood ("patch") sizes. Higher neighborhood sizes inidcates larger receptive field sizes. Higher values for C1 and C2 indicate feature richness. All C1 and C2 value ranges (x-axes) are z-normalized.

At layer C2, a template matching approach is used: The spatial orientations within each face/house image are fit to a set of prototypical composite features present within an independent set of natural images (see Methods). The median fit again quantifies the relative occurrence of these prototypical composite features within each face/house image and neighborhood (i.e., "patch" or receptive field) size. As at layer C1, we similarly found at C2 that house stimuli showed significantly higher median fits (i.e., lower Euclidian distance) to prototypical spatial features across different neighborhood sizes (Figure 3, right panel; see Methods for model details). Overall, these findings indicate that our house stimuli are much more feature rich than our face stimuli. Interestingly, although all *t*-tests exhibited strong effects, the degree of statistical differentiation between face and house conditions was greater for C1 than for C2. This highlights that primary/secondary visual cortex (V1/V2) may be particularly sensitive to such condition differences in visual feature density.

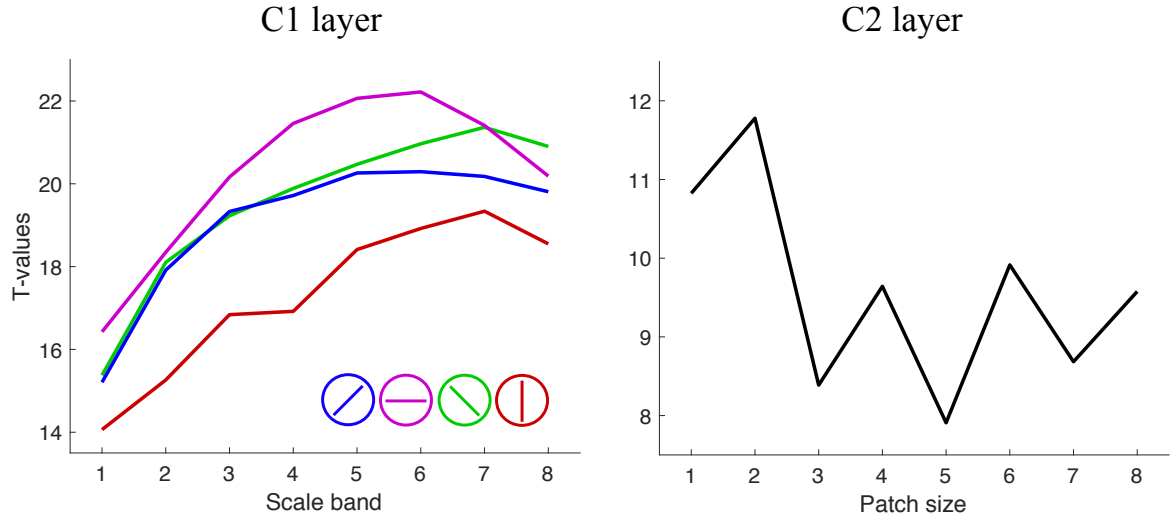

Figure 3: Independent sample t-test values for C1 and C2 layers. All t-values represent house minus face conditions. For C1, *t*-values are plotted *for each orientation and scale band;* associated *p*-value range = ~1.00* 10^{-22} to 10^{-32}. For C2, values are plotted for each patch size; associated *p*-value range = ~1.00* 10^{-12} to 10^{-21}. Equal variances not assumed for any test.

Multivariate model linking condition differences in fMRI-based temporal variability to offline behavior

Next, we examined whether greater within-person upregulation of brain signal variability was a marker of faster and more stable cognitive performance outside the scanner. In this way, we attempted to establish trait-based, latent-level relations between behavioral performance and one's ability to upregulate brain signal variability in line with environmental demands. To test this idea, we first ran a multivariate partial least squares (PLS) model linking upregulation of SD_{BOLD} from face to house (i.e., within-voxel data = house SD_{BOLD} minus face SD_{BOLD}) to speeded cognitive performance outside the scanner. A robust latent variable (permuted p = 0.048, accounting for 59.93% of the crossblock covariance) resulted, indicating that greater face to house upregulation of SD_{BOLD} predicted faster (on 8/9 measures) and more stable (7/9 measures) reaction time performance outside the scanner (see Figure 4, Figure S1 for full axial view, and Methods for full list of offline tasks, which were all visual in nature). All bar plots are also included as scatters in Figure S2. Spatially, this effect was most prominent in visual cortex (largely V1 and V2), and then in precuneus/posterior cingulate regions (see Table 1); fusiform face and parahippocampal place regions were not sensitive in our model. There were also no brain regions that showed the opposite effect (i.e., higher SD_{BOLD} on face

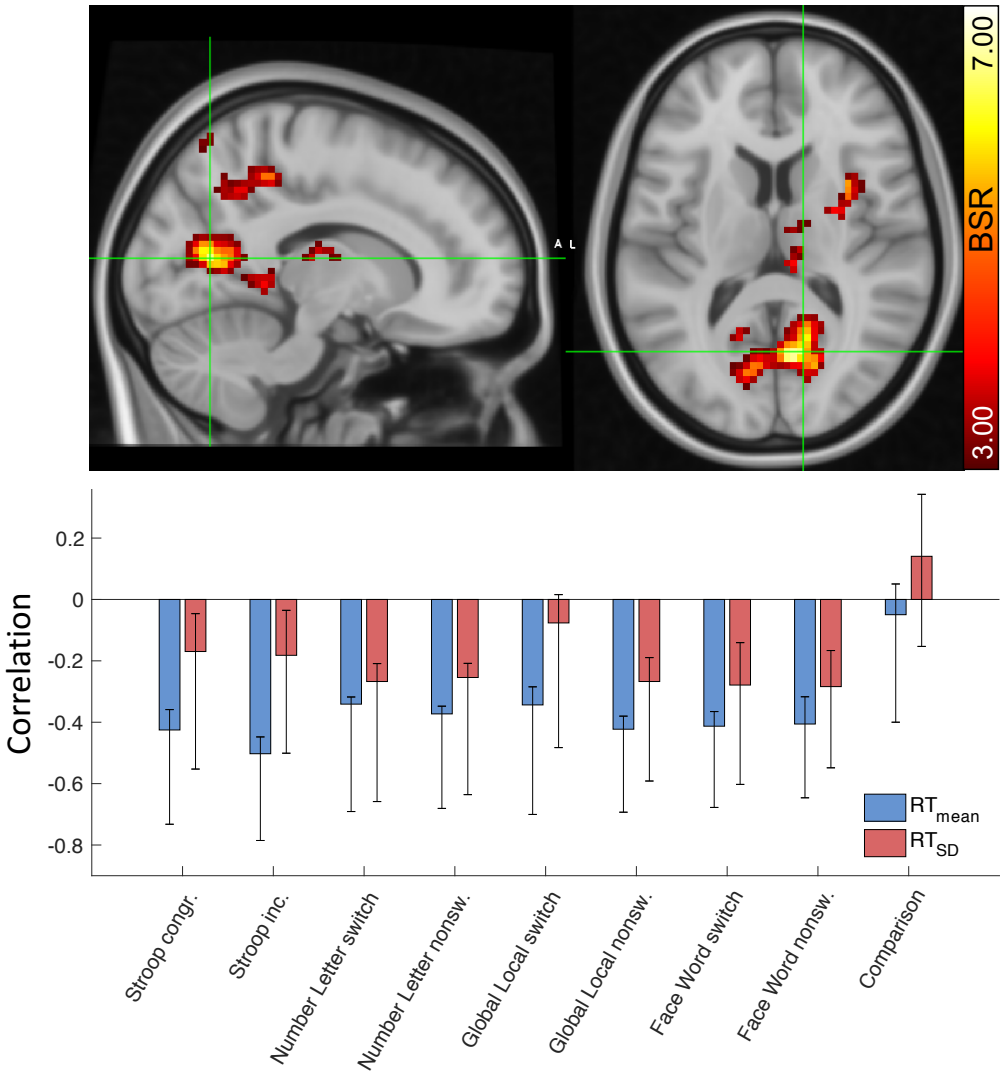

Figure 4: Multivariate model showing that greater SD_{BOLD} upregulation during house compared to face conditions (house_SD_{BOLD} minus face_SD_{BOLD}) correlates with faster and more stable offline performance. BSR = bootstrap ratio. Error bars represent 95% bootstrap confidence intervals of relations across 1000 resamples (with replacement) of the data.

Table 1: Multivariate PLS model peak activations, bootstrap ratios, and cluster sizes: Regions expressing heightened SD_{BOLD} on house vs face in relation to faster and more stable offline speeded performance. SD = standard deviation; BOLD = blood oxygen level-dependent; Hem = hemisphere; MNI = Montreal Neurological Institute; BSR = bootstrap ratio (model salience/bootstrapped standard error).

		MNI coordinates				Cluster size
Region	Hem	X	Y	Z	BSR	(voxels)
V1/V2	R	9	-69	15	6.35	687
Middle frontal gyrus	R	36	42	21	4.89	36
Insula	R	36	6	12	4.82	86
Superior occipital gyrus	L	-21	-75	39	4.46	92
Superior parietal lobule (area 5ci)	R	12	-42	48	4.45	193
Thalamus	R	9	-15	15	4.36	32

vs. house was never functionally relevant at the current bootstrap threshold level). Notably, greater upregulation of SD_{BOLD} from face to house not only correlated with better performance, but was also in line with significantly greater feature density in house compared to face conditions, as determined via the HMAX model (Figure 3).

Given that adult age has been found to be a major correlate of individual differences in SD_{BOLD} in previous studies[3,4], we therefore tested the above links between face-house upregulation of SD_{BOLD} and reaction time performance while controlling for chronological age. All effects in Figure 3 remained virtually identical (see Table S1 for age-partialled effects).

We also investigated the relation between SD_{BOLD} upregulation and behavioral accuracy; although greater SD_{BOLD} upregulation tended to be associated with higher accuracy, this effect was not significant at the latent level (first and strongest latent variable; permuted $p = .30$).

Typical $mean_{BOLD}$-based face-house condition differences are insensitive to offline performance

To compare our variability-upregulation findings to a more standard approach, we used an identical PLS modeling approach, but using voxel-wise $mean_{BOLD}$ instead of SD_{BOLD} as the neural measure of interest. This permitted comparison of relative sensitivity of both signal types in relation to offline performance. A behavioural PLS model linking condition differences in $mean_{BOLD}$ to offline speeded performance (N = 44; two extreme $mean_{BOLD}$ outliers were detected and removed that did not appear in the SD_{BOLD} models above) revealed no significant latent effect (permuted $p = .15$). Null findings also emerged when relating $mean_{BOLD}$ to offline accuracy (permuted $p = .22$). These results are in accord with previous work showing that SD_{BOLD} is more sensitive to individual differences in behavior than is $mean_{BOLD}$[5,19-21].

DISCUSSION

In the current study of healthy older adults, we found that temporal variability in BOLD was an excellent marker of task conditions (faces and houses) differing in level of visual input differentiation (determined via a feedforward computational model of the ventral visual stream (HMAX)). Critically, the more a subject upregulated SD_{BOLD} in line with stimulus feature richness (houses more than faces), the faster and more stable were their reaction times across a series of different offline speeded measures. Notably, this effect was most prominent in V1 and V2, the same regions thought to be functionally represented in the HMAX layers (particularly C1) within which houses were maximally more feature dense relative to faces. We also found that a typical $mean_{BOLD}$-based model did not relate to offline performance, lending further support to the principled examination of temporal fluctuations in brain signals in humans.

Various bases for elevated brain signal variability in response to more feature rich visual input

At least since the 1950s, various researchers have suggested that early visual regions actively work to reduce redundancy in stimulus content (e.g., via "redundancy filtering"[22,23]). In accord with such theories, the visual cortex often exhibits rapid ensemble-level suppression to more common (or expected) stimuli or stimulus trains, and greater ensemble-level response to more unexpected (or complex) stimuli[11-13]. This has important implications for BOLD

variability. Because we examined within-voxel temporal variability across trials and blocks for each stimulus category, and each voxel is a moment-to-moment ensemble-level approximation of synaptic/input activity over several million neurons, lower dynamic range of BOLD in response to more predictable/homogeneous stimulus categories such as faces may indeed reflect category-level ensemble synaptic/input suppression (or in general, "coding efficiency"). Conversely, more feature rich visual input (as for houses) should ensure that dynamic range of brain responses remains broader across the stimulus period. Indeed, Hermundstad et al.[24] argue that within-stimulus variance itself can *drive* salience, and that the visual system should thus upregulate allocated resources (perhaps expressed as dynamic range) to effectively encode more feature rich types of stimuli. The authors also showed that this effect occurs even via natural scene viewing in the absence of a specific task, similar to the use of passive viewing in the current fMRI study.

Notably, our findings also converge with computational and animal work (membrane potentials, spiking) suggesting that "perceptual uncertainty" can be probabilistically encoded by the variability of neural responses in visual cortex[10]. In particular, Orbán et al. predict that wider ranges of image features should indeed yield wider distributions of neural responses. They show, for example, that the variability of V1 responses over different types of stimuli (so-called "signal variability") increases with increasing sensory evidence (captured by contrast in the author's study). In the present study, stimuli that were more feature rich (houses) also yielded increased brain dynamics. Critically however, we show that individual differences in response to such stimulus input differentiation matter for trait-level behavior; older adults who expressed greater upregulation of BOLD signal variability in relation to stimulus variability were also faster and more stable in offline speeded behavior across a battery of tasks.

The Orbán et al. findings provide a potential bottom-up conceptualization of this general phenomenon (i.e., signal variability as a function of perceptual input). However, top-down effects may also be important in relation to the current phenomena. In particular, predictive coding models also offer a number of potential points of insight into the current results. Conceptualizations of predictive coding[14] generally presume that when neural priors for stimulus input are more "certain" (distributionally narrow), incoming stimuli within that category will also naturally be less "surprising" for the system, thus maintaining an already stable prior and making processing and prediction of future stimuli relatively easy. However, Mlynarski et al. make a critical distinction regarding uncertainty: "The degree to which incoming stimuli are surprising to the observer depends on two factors: the average surprise of the stimuli themselves, which is a property intrinsic to the stimulus distribution, and the alignment of the observer's belief with this stimulus distribution" (p. 4). Regarding the former, the authors then go on to state that: "High-variance stimuli will therefore be more surprising to an observer, on average, than low-variance stimuli" (p. 4-5).

It is this former type of uncertainty that seems most relevant to the current study. Faces are an excellent candidate for consideration as a relatively certain distribution/prior[25,26]. Humans are considered face experts in general relative to other stimulus categories[27,28], and faces can be reduced to a limited number of statistical dimensions, yet still be processed, discriminated, and recognized[29-31]. Accordingly, feature density in face stimuli also appeared particularly minimized at layer C1 in the present HMAX model results; this suggests that the relative lack of "simple" features in face stimuli may heighten the chance that faces remain more distributionally "certain" overall (or relatively non-updatable) for the brain, particularly in V1/V2. Indeed, Mlynarski et al. anticipate that the brain should be able to minimize metabolic costs and lessen neural dynamic range when processing such "reducible" types of stimuli. In

our data, this idea may be reflected in a relative dampening of the dynamic range of BOLD signal in the face condition.

However, house stimuli appear to be a much more feature rich stimulus category, and accordingly, one's prior for houses could conceivably also be relatively broad. Humans may know generally what constitutes a "house," but the compositional variations among house types is intuitively larger than for faces. Although predictive coding would assume that a relatively broad prior distribution for houses should adjust more rapidly to exposure to a surprising house, we would argue that it is unlikely that any natural prior distribution for houses will achieve the "certainty" humans express for faces. The brain may simply maintain broader priors for stimulus categories that are naturally more feature rich, and as predicted by Mlynarski et al.[14], the brain may require a greater dynamic range to process such stimuli. Because greater upregulation of SD_{BOLD} for houses was indicative of faster and more stable offline speeded performance on the vast majority of tasks examined, this suggests that maintaining similar neural dynamic ranges across stimulus categories despite naturally different levels feature density is an ineffective operational mode for the human brain. An effective brain may in fact need to continue to sample a dynamic and differentiated world (when required) to remain "optimal." Friston et al.[32] make a key related argument, that the brain should not fix its solutions too rigidly, instead allowing for maintenance of neural itinerancy (or instability) to approximate or maintain Bayes-optimal perception. Although fitting narrow solutions for relatively undifferentiated stimulus categories may be functional or even "optimal," the most adaptable brain should also be "meta-variable," and invoke differentiated levels of dynamic range to prepare and/or respond to more differentiated levels of dynamic input as required.

Relatedly, Marzen and DeDeo[33] argue in their computational work that well-adapted organisms should be able to use both (1) a low-fidelity encoding regime wherever perceptual costs can be minimized, and (2) a high-fidelity mode during which perceptual costs increase with environmental complexity. In our study, such fidelity modes appear to be reflected in the variability of brain activity (thus fitting our notion of "meta-variability" to differential visual feature densities in high performers). This suggests that in more feature rich environments, high performers may do well because they can upregulate "fidelity" to allow them to encode key distinctions in their environment.

Limitations and next steps

In an effort to describe the relative feature richness within face and house stimuli, we quantified median within-image C1 and C2 layer features (see Figure 1 and 2). However, visual inspection of stimulus categories in Figure 2 highlights the presence of greater item-wise differentiation in houses compared to faces (at least clearly at layer C1). Because SD_{BOLD} is computed across TRs and stimuli within-condition, our findings could represent a hybrid of variable responses at within- and between-item levels within each condition. However, notably large *t*-values (Figure 3) suggest that condition differences in median feature richness remain key. Faster imaging methods (EEG/MEG) are needed in future work to disentangle the relative influence of within- and between-item differences on brain signal variability levels, despite the loss of spatial information such techniques would impose.

Another limitation of the current study was that the sample was relatively healthy and age homogeneous (59-73 years). Although this narrow age range helps assuage concerns regarding vascular differences that may play a role in extreme age group comparisons of BOLD variability[34,35], future work could expand to examine whether (a) the highest

performing older adults in the current sample approach young adult levels in SD_{BOLD} face-house upregulation in the same behaviourally-relevant brain regions (i.e., "maintenance"[36]), or whether (b) spatial expressions of these effects qualitatively differ. Finally, although trait-level individual difference arguments are possible from the current results given the link between within-scanner brain signal variability and offline speeded performance, related follow-up work would benefit from quantifying behaviour while simultaneously undergoing neuroimaging (e.g., to achieve more stringent tests of candidate predictive coding models). Evidence for individual differences in the coupling between signal variability and density of sensory input would only be strengthened if ongoing and instantaneous responses to differing stimulus input could be behaviorally quantified within- and across trials (e.g., via methods that allow faster temporal sampling, such as EEG or MEG).

Conclusion

We found that greater within-person upregulation of brain signal variability in response to more feature-rich visual input was a robust marker of faster and more stable behavioural performance in healthy older adults. Such "meta-variability" to differential stimulus inputs may thus reflect trait-level performance optimality.

METHODS

Computational model

Estimation of stimulus feature differentiation via a feedforward model of the ventral visual system (HMAX)

In the current fMRI task design, participants passively viewed 60 face and 60 house stimuli in blocks of 15 trials. To model visual feature density in these images, we submitted each image to the HMAX feedforward model of the ventral visual system[15,17] (code is freely available at: http://maxlab.neuro.georgetown.edu/hmax.html). All four model layers are depicted in Figure 1. Layers S1 and C1 correspond to V1/V2 function, and layers S2 and C2 to V2/V4 function[16]. Within the first layer (S1), a range of Gabor filters (intended to provide a principled model of cortical simple cell receptive fields, with 16 different filters corresponding to *n* x *n* pixel neighborhoods (sizes: [7:2:37])) and four orientations (HMAX defaults: -45°, 0°, 45°, 90°) are fitted to each image in overlapping windows (50% overlap). The resulting S1 map corresponds to simple cell responses for all positions within the input image, and the fitting procedure is completed for each orientation and filter size separately (see example filter sizes of 11x11 and 13x13 in Figure 1).

At the next layer (complex cells in C1), two consecutive maximization steps over S1 simple cells are computed: (1) over two neighboring filter sizes for each S1 cell, and then (2) over a pool of S1 cells. Because 16 filter sizes are used in HMAX [7:2:37 pixels], taking the max over neighboring pairs of filters results in eight "scale bands". The scale band index then determines the spatial neighborhood of S1 cells over which is pooled in the second step [8:2:22 S1 cells], independently for each orientation[17]. We took the median C1 value within each image, for each scale band and orientation separately. We then compared these within-image median values, within each scale band and orientation, between face and house stimuli. This resulted in 8x4 independent sample t-tests (equal variances not assumed; see Figure 3, left panel).

At the third layer (S2, composite feature cells), a template-based approach is used to estimate the fit to simple and complex (hybrid) C1-level prototypical feature sets included in the HMAX code, and derived from a library of naturalistic stimuli[17]. Eight different C1 neighborhood sizes [2:2:16] for each of 400 different features were fitted. S2 cells pool over C1 cells within each neighborhood and scale band (but across all orientations), quantifying the fit between the spatial features of the input image and those of the stored prototypes[17].

The final layer (C2, complex composite feature cells) then takes the max over all scale bands, quantifying the global fit (inverse Euclidean distance) between the features of each image and each prototype, separately for each prototype C1 neighborhood size. When comparing face and house stimuli, we took the median fit per image for each C1 neighborhood size separately, resulting in eight independent samples t-tests (equal variances not assumed, see Figure 3, right panel).

fMRI experiment

Participants

The initial sample utilized in the current study consisted of 48 community-dwelling older adults aged 59-73 (mean 66.05 ± 4.40, 30 female), and represent the pre-training sample from a sample described previously[37,38]. All participants had MMSE score ≥ 26, were free of neurological, psychiatric, and cardiovascular diseases, were right-handed, and were suitable for MR assessment (e.g. no magnetic implants, no claustrophobia). This study was carried out in accordance with the recommendations of the ethics committee of the German Psychological Society. All participants gave written informed consent in accordance with the Declaration of Helsinki and participated voluntarily. They were paid for study completion. Two subjects were discarded from the current sample, one with improper slice positioning during scanning, and another was an extreme outlier on the Stroop task (an offline speeded measure; see below). Thus, analyses were based primarily on data from 46 participants (unless otherwise specified in text).

MRI Data Acquisition, Task, Preprocessing, and Analyses

Brain images were acquired on a Siemens TIM Trio 3T MRI scanner (Siemens, Erlangen, Germany) at the Max Planck Institute for Human Development in Berlin. A high-resolution T1-weighted MPRAGE (TR = 2500 ms, TE = 4.76 ms, TI = 1100 ms, flip angle = 7°, acquisition matrix = 256 × 256 × 176, 1 mm isotropic voxels) was first acquired. A conventional echo-planar MR sequence was then used for functional acquisitions (TR = 2000 ms, TE = 30 ms, flip angle = 80°, FOV = 216mm) encompassing 192 volumes per run and 36 slices per volume (slice thickness 3 mm). Slices were 72×72 matrices acquired parallel to the Corpus Callosum.

During functional imaging, participants passively viewed greyscale face, house, or phase-scrambled face/house images (following the procedures of [1]) across two runs, each of which consisted of four blocks per stimulus category. Each block contained 15 images shown for 2 seconds each, resulting in 30 second block lengths (total of 6 minutes per run). Stimuli were presented via E-prime (Psychology Software Tools, Pittsburgh, PA) and displayed by a projection system.

fMRI data were preprocessed with FSL 5[39,40]. Pre-processing included motion-correction with spatial smoothing (7 mm full-width at half maximum Gaussian kernel) and bandpass filtering (.01-.10 Hz). We registered functional images to participant-specific T1 images, and from T1

to 2mm standard space (MNI 152_T1) using FLIRT. We then masked the functional data with the GM tissue prior provided in FSL (thresholded at probability > 0.37). We detrended the data (up to a cubic trend) using the SPM_detrend function in SPM8. We also utilized extended preprocessing steps to further reduce data artifacts[5,19,20]. Specifically, we subsequently examined all functional volumes for artifacts via independent component analysis (ICA) within-run, within-person, as implemented in FSL/MELODIC[41]. Noise components were identified according to several key criteria: a) Spiking (components dominated by abrupt time series spikes); b) Motion (prominent edge or "ringing" effects, sometimes [but not always] accompanied by large time series spikes); c) Susceptibility and flow artifacts (prominent air-tissue boundary or sinus activation; typically represents cardio/respiratory effects); d) White matter (WM) and ventricle activation[42]; e) Low-frequency signal drift[43]; f) High power in high-frequency ranges unlikely to represent neural activity (≥ 75% of total spectral power present above .10 Hz;); and g) Spatial distribution ("spotty" or "speckled" spatial pattern that appears scattered randomly across ≥ 25% of the brain, with few if any clusters with ≥ 80 contiguous voxels [at 2x2x2 mm voxel size]). Examples of these various components we typically deem to be noise can be found in supplementary materials in Garrett et al.[21] By default, we utilized a conservative set of rejection criteria; if manual classification decisions were challenging due to mixing of "signal" and "noise" in a single component, we generally elected to keep such components. Three independent raters of noise components were utilized; > 90% inter-rater reliability was required on separate data before denoising decisions were made on the current data. To enable semi-automated data denoising using FSL FIX, we manually classified 30% of participant data to provide a noise component training set. Features from the noise component training set were then extracted, and used to detect noise components from the remaining 70% of participant data via FIX. Upon evaluating the automated labelling for several subjects against our manual decisions, we used a FIX threshold of 60, which permitted a best match to manual decisions of two independent raters. Components identified as artifacts were then regressed from corresponding fMRI runs using the *regfilt* command in FSL. We found previously that these additional preprocessing steps had dramatic effects on the predictive power of SD_{BOLD} in past research, effectively removing 50% of the variance still present after traditional preprocessing steps, while simultaneously doubling the predictive power of SD_{BOLD}[20]. Critically, our recent work also suggests that when such denoising approaches are applied, age differences in SD_{BOLD} remain robust to multiple vascular controls measured via dual-echo ASL-BOLD using carbogen-based hypercapnia[34]. The present sample only contains a narrow age range of older adults (59-73 years), further minimizing the potential impact of aging-based differences in vasculature. For all robust models presented in the current paper, we also partial chronological age from all effects to further confirm that any residual (post-denoising) age-related artifacts are controlled (see Results and Table S1).

Voxel-wise estimates of SD_{BOLD} and comparison to $mean_{BOLD}$

To calculate SD_{BOLD}, we first performed a block normalization procedure to account for residual low frequency artifacts. We normalized all blocks for each condition such that the overall 4D mean across brain and block was 100. For each voxel, we then subtracted the block mean and concatenated across all blocks. Finally, we calculated voxel standard deviations across this concatenated time series[20]. All models described below were run on grey matter (GM) only, after a standard GM mask derived from the MNI152 average brain was applied to each 4D image set.

We sought also to compare SD_{BOLD} results to a typical mean-based measure of BOLD activity ($mean_{BOLD}$). We calculated mean signal ($mean_{BOLD}$) for each experimental condition as follows; we first expressed each signal value as a percent change from the average of the last

four scans from the previous block, and then calculated a mean percent change within each block and averaged across all blocks for a given condition (a typical method in the PLS data-analysis framework). This effectively acts as an explicit high-pass filter over the data. We then re-ran relevant PLS models described below, while using $mean_{BOLD}$ measures.

Statistical modeling: Partial Least Squares

To examine multivariate relations between SD_{BOLD} face-house upregulation and offline speeded performance, we utilized behavioural PLS analysis[44,45]. This modelling form begins by calculating a between-subject correlation matrix (CORR) between (1) each voxel's SD_{BOLD} upregulation value (i.e., house SD_{BOLD} minus face SD_{BOLD}) and (2) a series of offline cognitive measures (either RT or accuracy based, depending on model (see Results and Supplemental Materials). CORR is then decomposed using singular value decomposition (SVD).

$$SVD_{CORR} = USV'$$

This decomposition produces a left singular vector of offline task weights (U), a right singular vector of brain voxel weights (V), and a diagonal matrix of singular values (S). A single estimable latent variable (LV) results that represents the relations between performance and SD_{BOLD} upregulation values. This LV contains a spatial activity pattern depicting the brain regions that show the strongest relation to offline performance identified by the LV. Each voxel weight (in V) is proportional to the voxel-wise correlation between voxel offline behaviour and SD_{BOLD}.

Significance of detected relations was assessed using 1000 permutation tests of the singular value corresponding to the LV. A subsequent bootstrapping procedure revealed the robustness of within-LV voxel saliences across 1000 bootstrapped resamples of the data[46]. By dividing each voxel's weight (from V) by its bootstrapped standard error, we obtained "bootstrap ratios" (BSRs) as normalized estimates of robustness. For the whole brain analysis, we thresholded BSRs at values of ±3.00 (which exceeds a 99% confidence interval; see Figure 2).

We also obtained a summary measure of each participant's robust expression of a particular LV's spatial pattern (a within-person "brain score") by multiplying the model-based vector of voxel weights (V) by each subject's vector of voxel SD_{BOLD} upregulation values (Q), producing a single within-subject value,

$$\text{Brain score} = VQ'$$

Offline visuocognitive assessment

Participants completed a 90-minute cognitive testing session outside the scanner. For the current study, the cognitive battery spanned the following six cognitive abilities: perceptual speed, inhibition, switching, updating, episodic memory, and reasoning. Responses for computerized tasks were provided via response boxes or the computer keyboard. A total of 16 tasks were administered, but for the current study, only nine were considered. First, we examined all tasks for (1) RT and (2) accuracy models as a function of: (a) initial inspection of normality of between subject distributions for each task variable; (b) if necessary, successful transformation of non-normal distributions to Gaussian (either via log or square root transformation, and examined via a combination of Kolmogorov-Smirnov test for normality and Q-Q plot for each variable), and; (c) consideration for whether speed or accuracy was emphasized to participants. The following choices of variables resulted.

RT-based measures

For each variable, all trials in which RT was < 200 ms or greater than ±3 SDs from within-person means were dropped prior to computing reaction time means (RT_{mean}) and SDs (RT_{sd}) for each subject. RT measures were only computed for correct trials for all tasks.

Inhibition was assessed via the Stroop task (Stroop, 1935); color-words were shown in either the same (congruent) or different (incongruent) colored font in the center of the screen for 1000 ms. Participants were asked to indicate as quickly as possible the font color; the next stimulus only appeared 1000 ms after an answer was given. Participants completed 24 practice trials and four blocks of 36 test trials each; 50 % of trials were incongruent (color-word and font color did not match).

Task switching was assessed using three tasks: the number-letter task (Rogers and Monsell, 1995), the global-local task (Kinchla et al., 1983) and the face-word task (Yeung et al., 2006). During the number-letter task, participants saw a number-letter pair appearing in one of four quadrants of the screen (top left, top right, bottom left, bottom right). In cases where the stimulus pair appeared at the top, participants had to attend to the number, and indicate whether it was odd or even. If the stimulus pair appeared at the bottom, participants were instructed to attend to the letter, and indicate whether it was a vowel or a consonant. Stimuli included 2, 3, 4, 5, 6, 7, 8, 9, A, E, I, U, G, K, M, R. For the global-local task, participants were presented with Navon figures, i.e. large objects composed of small objects. Objects were always circles, triangles, squares, or crosses, e.g. a large circle composed of small triangles. If the objects appeared in blue, participants had to indicate the shape of the larger (global) object. If the objects appeared in black, participants had to indicate the shape of the smaller (local) objects. During the face-word task, participants saw 1-or 2-syllable words overlaid on male or female faces. A key appeared below the stimulus pair, indicating whether the face or the word should be attended. For words, participants were required to indicate whether the word had one or two syllables, whereas for faces they had to decide whether it was female or male. For all task-switching tasks, stimuli were presented for 2500 ms and the next stimulus only appeared 500 ms after an answer was given via response boxes. Trials were randomly presented, with 50 % of the trials requiring a task-switch. For every task, participants completed 24 practice trials followed by 128 test trials, divided into four separate blocks of 32 trials each.

Perceptual speed was assessed using the figural comparison test (Schmiedek et al., 2010). On each trial, participants saw two colored, three-dimensional objects side-by-side on a computer screen for a maximum of 5000 ms, and were instructed to decide as quickly as possible whether the objects were identical. Responses were provided via response boxes and the stimuli disappeared as soon as an answer was given or after 5000 ms. Five-hundred ms thereafter the next object pair appeared. Following 20 practice trials, participants completed 40 test trials.

Because our goal was to examine latent level relations between SD_{BOLD} and offline speeded performance, we examined multiple estimates from the tasks above. In particular, for Stroop and all task switching tasks, two estimates each were taken: Stroop (congruent and incongruent), and separate estimates from switch and non-switch trials for number-letter, global-local, and face-word. In favour of examining latent level speeded performance across domains, we do not consider congruency (Stroop) or switch costs directly here, which explicitly capture the difference (rather than similarity) between trial types.

Accuracy-based measures

We assessed updating using three different tasks: letter updating, spatial updating and 2-back (all taken from Schmiedek et al., 2009). During letter updating, single letters (A, B, C, or D) appeared randomly on the screen one after the other for 2500 ms with a 500 ms ISI. The presentation sequence stopped after 7, 9, 11, or 13 letters and the task instructed participants to enter the last three letters displayed, via the computer keyboard. After four practice trials, participants completed two sequences composed of 7, 9, 11, or 13 letters each, resulting in a total of eight trials presented in randomized order. During spatial updating, participants were shown two 3 × 3 grids, presented side-by-side on the computer screen. At the beginning of every trial, a dot appeared simultaneously in each grid for 4000 ms and participants were instructed to remember the position of the dot. Next, arrows appeared synchronously above each grid for 2500 ms, indicating that the dot in the respective grid had to be moved one field in the direction of the arrow. After 500 ms another pair of arrows required another moving of the dots. At the end, the final position of the dots had to be marked in the grids via mouse click. After a practice trial, participants completed two easy trials including two updating operations per grid, as well as two difficult trials including three updating operations per grid. During the 2-back, single digits (1-9) appeared randomly on the screen for 500 ms one after the other with a ISI of 3000 ms. Participants were asked to indicate, whether the currently presented digit was identical to the digit presented two displays earlier in the sequence or not. After one practice sequence (26 numbers), participants completed three test sequences (39 numbers).

Finally, reasoning was assessed using a version of Raven's progressive matrices (Raven et al., 1998). Participants saw a 3 × 3 matrix with patterns following certain regularities. The pattern on the lower right was missing, and participants were instructed to identify the correct pattern out of eight given alternatives. A total of 15 trials could be completed within a maximum of 15 minutes. For all four tasks, accuracy served as outcome measure.

Acknowledgements

D.D.G was supported by an Emmy Noether Programme grant from the German Research Foundation. U.L. acknowledges financial support from the Intramural Innovation Fund of the Max Planck Society. D.D.G and U.L. were also partially supported by the Max Planck UCL Centre for Computational Psychiatry and Ageing Research. Finally, we would like to thank Martin Hebart for helpful discussions regarding implementation of HMAX.

References

1. Park, J., Carp, J., Hebrank, A., Park, D. C. & Polk, T. A. Neural Specificity Predicts Fluid Processing Ability in Older Adults. *J. Neurosci.* **30,** 9253–9259 (2010).
2. Carp, J., Gmeindl, L. & Reuter-Lorenz, P. A. Age Differences in the Neural Representation of Working Memory Revealed by Multi-Voxel Pattern Analysis. *Front Hum Neurosci* **4,** (2010).
3. Garrett, D. D. *et al.* Moment-to-moment brain signal variability: A next frontier in human brain mapping? *Neuroscience & Biobehavioral Reviews* **37,** 610–624 (2013).
4. Grady, C. L. & Garrett, D. D. Understanding variability in the BOLD signal and why it matters for aging. *Brain Imaging and Behavior* **8,** 274–283 (2013).
5. Garrett, D. D. *et al.* Amphetamine modulates brain signal variability and working memory in younger and older adults. *Proc. Natl. Acad. Sci. U.S.A.* **112,** 7593–7598 (2015).
6. Garrett, D. D., Kovacevic, N., McIntosh, A. R. & Grady, C. L. The Modulation of BOLD Variability between Cognitive States Varies by Age and Processing Speed. *Cereb. Cortex* **23,** 684–693 (2012).
7. Knill, D. C. & Pouget, A. The Bayesian brain: the role of uncertainty in neural coding and computation. *Trends in Neurosciences* **27,** 712–719 (2004).
8. Beck, J. M. *et al.* Probabilistic Population Codes for Bayesian Decision Making. *Neuron* **60,** 1142–1152 (2008).
9. Ma, W. J., Beck, J. M., Latham, P. E. & Pouget, A. Bayesian inference with probabilistic population codes. *Nature Neuroscience* **9,** 1432–1438 (2006).
10. Orbán, G., Berkes, P., Fiser, J. & Lengyel, M. Neural Variability and Sampling-Based Probabilistic Representations in the Visual Cortex. *Neuron* **92,** 530–543 (2016).
11. Vinken, K., Vogels, R. & Op de Beeck, H. Recent Visual Experience Shapes Visual Processing in Rats through Stimulus-Specific Adaptation and Response Enhancement. *Current Biology* **27,** 914–919 (2017).
12. Hamm, J. P. & Yuste, R. Somatostatin Interneurons Control a Key Component of Mismatch Negativity in Mouse Visual Cortex. *Cell Reports* **16,** 597–604 (2016).
13. Homann, J., Koay, S. A., Glidden, A. M., Tank, D. W. & Berry, M. J., II. Predictive Coding of Novel versus Familiar Stimuli in the Primary Visual Cortex. *BioRxiv* doi:10.1101/197608
14. Mlynarski, W. & Hermundstad, A. M. Adaptive coding for dynamic sensory inference. *BioRxiv* (2017). doi:10.1101/189506
15. Riesenhuber, M. & Poggio, T. Hierarchical models of object recognition in cortex. *Nature Neuroscience* **2,** 1019–1025 (1999).
16. Serre, T. *et al.* A Theory of Object Recognition: Computations and Circuits in the Feedforward Path of the Ventral Stream in Primate Visual Cortex. *AI Memo -CBCL Memo* (2005).
17. Serre, T., Wolf, L., Bileschi, S., Riesenhuber, M. & Poggio, T. Robust object recognition with cortex-like mechanisms. *IEEE Trans. Pattern Anal. Machine Intell.* **29,** 411–426 (2007).
18. Serre, T., Oliva, A. & Poggio, T. A feedforward architecture accounts for rapid categorization. *Proc. Natl. Acad. Sci. U.S.A.* **104,** 6424–6429 (2007).
19. Garrett, D. D., Kovacevic, N., McIntosh, A. R. & Grady, C. L. The Importance of Being Variable. *J. Neurosci.* **31,** 4496–4503 (2011).
20. Garrett, D. D., Kovacevic, N., McIntosh, A. R. & Grady, C. L. Blood Oxygen Level-Dependent Signal Variability Is More than Just Noise. *J. Neurosci.* **30,** 4914–4921 (2010).
21. Garrett, D. D., McIntosh, A. R. & Grady, C. L. Brain Signal Variability is

Parametrically Modifiable. *Cereb. Cortex* **24,** 2931–2940 (2013).
22. van Hateren, J. H. A theory of maximizing sensory information. *Biol Cybern* **68,** 23–29 (1992).
23. van Hateren, J. H. Spatiotemporal contrast sensitivity of early vision. *Vision Res.* **33,** 257–267 (1993).
24. Hermundstad, A. M. *et al.* Variance predicts salience in central sensory processing. *Elife* **3,** 308 (2014).
25. Brodski, A., Paasch, G. F., Helbling, S. & Wibral, M. The Faces of Predictive Coding. *J. Neurosci.* **35,** 8997–9006 (2015).
26. Brodski-Guerniero, A. *et al.* Information-Theoretic Evidence for Predictive Coding in the Face-Processing System. *J. Neurosci.* **37,** 8273–8283 (2017).
27. Carey, S., Schonen, S. D. & Ellis, H. D. Becoming a Face Expert [and Discussion]. *Philos. Trans. R. Soc. Lond., B, Biol. Sci.* **335,** 95–103 (1992).
28. Carey, S. & Diamond, R. From piecemeal to configurational representation of faces. *Science* **195,** 312–314 (1977).
29. Sirovich, L. & Kirby, M. Low-dimensional procedure for the characterization of human faces. *J. Opt. Soc. Am. A* **4,** 519 (1987).
30. O'Toole, A. J., Abdi, H., Deffenbacher, K. A. & Valentin, D. Low-dimensional representation of faces in higher dimensions of the face space. *J. Opt. Soc. Am. A* **10,** 405 (1993).
31. Tsao, D. Y. & Livingstone, M. S. Mechanisms of Face Perception. *Annu. Rev. Neurosci.* **31,** 411–437 (2008).
32. Friston, K., Breakspear, M. & Deco, G. Perception and self-organized instability. *Front. Comput. Neurosci.* **6,** (2012).
33. Marzen, S. E. & DeDeo, S. The evolution of lossy compression. *Journal of The Royal Society Interface* **14,** 20170166 (2017).
34. Garrett, D. D., Lindenberger, U., Hoge, R. D. & Gauthier, C. J. Age differences in brain signal variability are robust to multiple vascular controls. *Sci. Rep.* **7,** 610 (2017).
35. D'Esposito, M., Deouell, L. Y. & Gazzaley, A. Alterations in the BOLD fMRI signal with ageing and disease: a challenge for neuroimaging. *Nat Rev Neurosci* **4,** 863–872 (2003).
36. Nyberg, L., Lövdén, M., Riklund, K., Lindenberger, U. & Bäckman, L. Memory aging and brain maintenance. *Trends Cogn Sci* **16,** 292–305 (2012).
37. Kleemeyer, M. M. *et al.* Exercise-Induced Fitness Changes Correlate with Changes in Neural Specificity in Older Adults. *Front Hum Neurosci* **11,** 791 (2017).
38. Kleemeyer, M. M. *et al.* Changes in fitness are associated with changes in hippocampal microstructure and hippocampal volume among older adults. *NeuroImage* **131,** 155–161 (2016).
39. Smith, S. M. *et al.* Advances in functional and structural MR image analysis and implementation as FSL. *NeuroImage* **23,** S208–S219 (2004).
40. Jenkinson, M., Beckmann, C. F., Behrens, T. E. J., Woolrich, M. W. & Smith, S. M. FSL. *NeuroImage* **62,** 782–790 (2012).
41. Beckmann, C. F. & Smith, S. M. Probabilistic Independent Component Analysis for Functional Magnetic Resonance Imaging. *IEEE Trans Med Imaging* **23,** 137–152 (2004).
42. Birn, R. M. The role of physiological noise in resting-state functional connectivity. *NeuroImage* **62,** 864–870 (2012).
43. Smith, A. M. *et al.* Investigation of Low Frequency Drift in fMRI Signal. *NeuroImage* **9,** 526–533 (1999).
44. McIntosh, A. R., Bookstein, F. L., Haxby, J. V. & Grady, C. L. Spatial Pattern Analysis of Functional Brain Images Using Partial Least Squares. *NeuroImage* **3,** 143–

157 (1996).

45. Krishnan, A., Williams, L. J., McIntosh, A. R. & Abdi, H. Partial Least Squares (PLS) methods for neuroimaging: A tutorial and review. *NeuroImage* **56,** 455–475 (2011).
46. Efron, B. & Tibshirani, R. J. in *An Introduction to the Bootstrap* 1–9 (Springer US, 1993). doi:10.1007/978-1-4899-4541-9_1

Supplemental Materials

	Stroop congruent	Stroop incongruent	Number Letter switch	Number Letter non-switch	Global Local switch	Global Local non-switch	Face Word switch	Face Word non-switch	Comparison
RT_{mean}	-.43/-.44	-.50/-.55	-.34/-.34	-.37/-.38	-.34/-.35	-.42/-.43	-.41/-.41	-.41/-.41	-.05/-.04
RT_{SD}	-.17/-.16	-.18/-.18	-.27/-.26	-.25/-.25	-.08/-.06	-.27/-.26	-.28/-.28	-.28/-.28	.14/.14

Table S1: Control for chronological age (via partial correlation) has no impact on relations between SD_{BOLD} upregulation and offline speeded performance on a series of visual tasks. Values represent original (left side of slash) and partial correlations (controlling for age; right side of slash) between latent-level upregulation (from face to house) in SD_{BOLD} and nine offline speeded task measures. $Mean_{RT}$ and SD_{RT} based relations are depicted. "Original" values are equivalent to those depicted in Fig 2 and Fig S2. Due to the numerical similarity between original and age-partialled results here, statistical tests of the difference were uninformative.

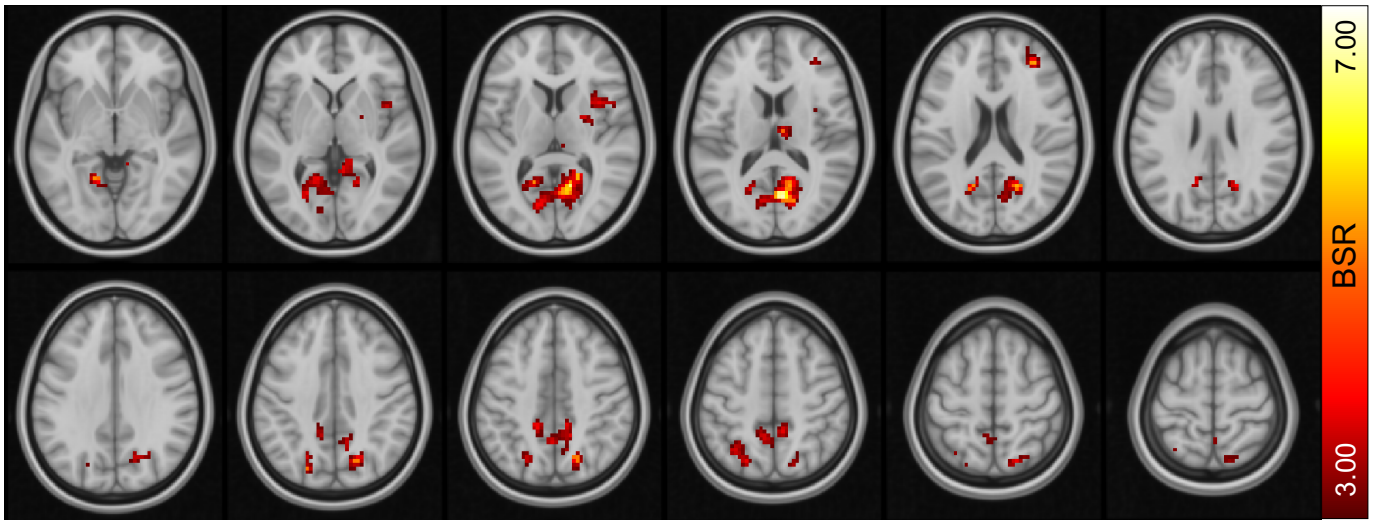

Figure S1: Axial slice representation of SD_{BOLD} upregulation – speeded performance multivariate effect depicted in Figure 3. Slices are shown from Z = -4 to Z = 62. BSR = bootstrap ratio. Left is left.

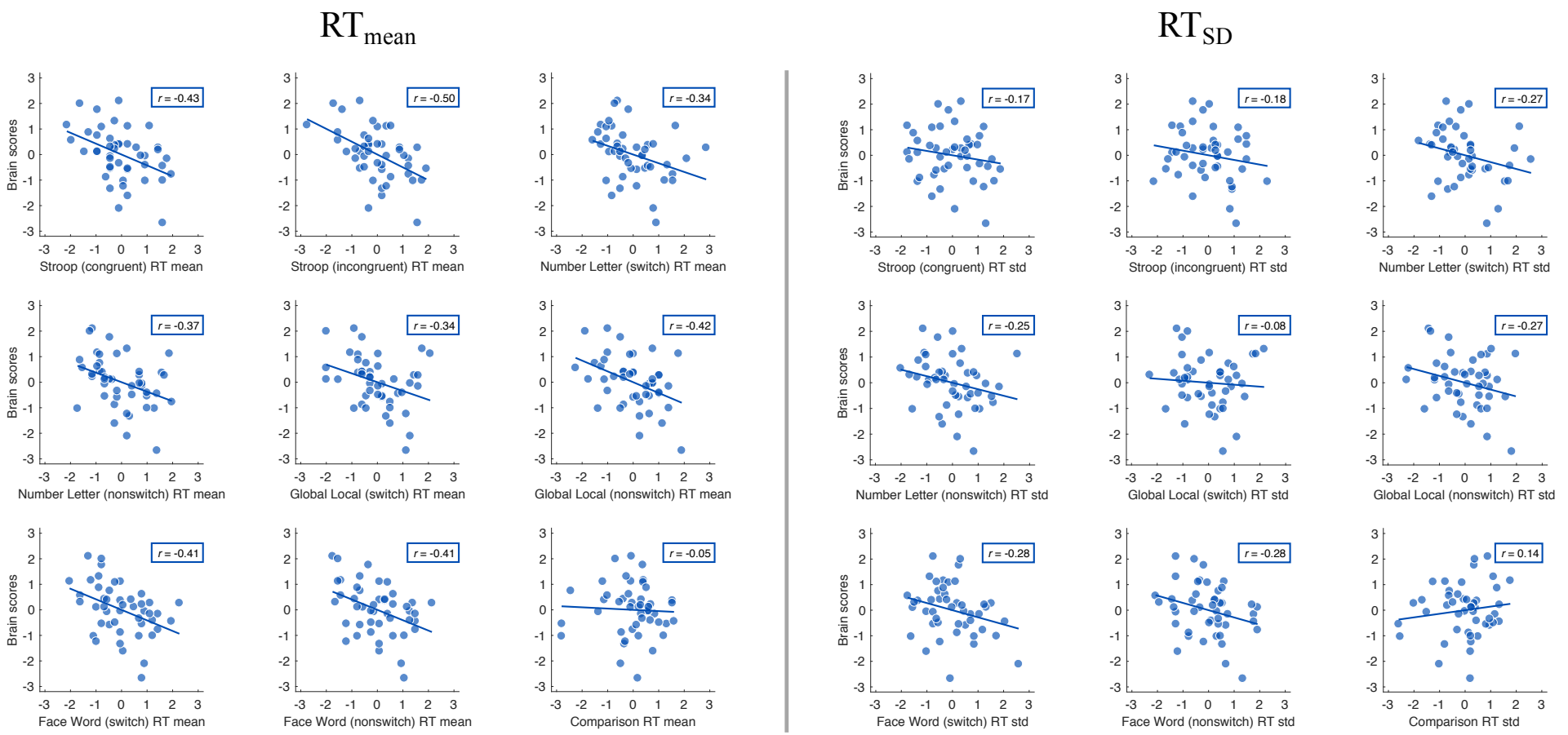

Figure S2: Dominant negative relations between face-house upregulation of SD_{BOLD} and offline speeded performance (RT_{mean} and RT_{SD}) on a series of visual tasks. All RT variables (x-axes) are log transformed, and all variables (x- and y-axes) are Z-transformed.